Inorganic Chemistry

Role of the Phosphine Ligands on the Stabilization of Monoadducts of the Model Nucleobases 1-Methylcytosine and 9-Methylguanine in Platinum(II) Complexes

Diego Montagner,[†] Ennio Zangrando,[‡] and Bruno Longato*,[†]

Dipartimento di Scienze Chimiche, Universitá di Padova, Via Marzolo 1, 35131 Padova, Italy, and Dipartimento di Scienze Chimiche, Universitá di Trieste, Via Giorgieri 1, 34127 Trieste, Italy

The addition of 1-methylcytosine (1-MeCy) or 9-methylguanine (9-MeGu) to solutions of *cis*-(PPh$_3$)$_2$Pt(ONO$_2$)$_2$ (**1a**), in a molar ratio of 1:1, affords the monoadducts *cis*-[(PPh$_3$)$_2$Pt(1-MeCy)(ONO$_2$)]NO$_3$ (**2a**) and *cis*-[(PPh$_3$)$_2$Pt(9-MeGu)(ONO$_2$)]NO$_3$ (**3a**) and only trace amounts of the bisadducts *cis*-[(PPh$_3$)$_2$Pt(1-MeCy)$_2$](NO$_3$)$_2$ (**4a**) and *cis*-[(PPh$_3$)$_2$Pt(9-MeGu)$_2$](NO$_3$)$_2$ (**5a**), respectively. The X-ray structural determination of **2a** and **3a** indicates a strong $\pi-\pi$ stacking interaction between one of the PPh$_3$ phenyl groups and the pyrimydinic N3-platinated cytosine or the imidazole part of the N7-coordinated guanine base. The addition of a further equiv of nucleobase to the monoadducts forms quantitatively the bisadducts that have been isolated as pure compounds **4a** and **5a**. Under the same experimental conditions, the dinitrato analogue *cis*-[(PMePh$_2$)$_2$Pt(ONO$_2$)$_2$] (**1b**) forms the monoadducts **2b** and **3b** in equilibrium with a relatively high concentration (20–30%) of the bisadducts *cis*-[(PMePh$_2$)$_2$Pt(1-MeCy)$_2$](NO$_3$)$_2$ (**4b**) and *cis*-[(PMePh$_2$)$_2$Pt(9-MeGu)$_2$](NO$_3$)$_2$ (**5b**), which have been structurally characterized by single-crystal X-ray analysis. The characterization of the isolated complexes by multinuclear NMR spectroscopy is also described.

Introduction

In the last 40 years, the interactions of model nucleobases with metal ions have been studied in great detail, in particular toward Pt^{II} centers having amine or diamine as ancillary ligands.[1] Recently, we have demonstrated that the use of monodentate phosphines (PR$_3$) as ligands led to the formation of platinum(II) complexes in which the nuclearity of the adducts and/or the binding mode of the nucleobase appear to depend on the nature of the substituents R on the phosphorus atoms. For instance, deprotonation of 9-substituted adenine (9-MeAd) promoted by the hydroxo complexes *cis*-[L$_2$Pt(μ-OH)]$_2$(NO$_3$)$_2$ affords the dinuclear species *cis*-[L$_2$Pt{9-MeAd(-H)-N^1N^6}]$_2$(NO$_3$)$_2$ when L is PMe$_3$[2] and the trinuclear adducts *cis*-[L$_2$Pt{9-MeAd(-H)-N^1N^6}]$_3$(NO$_3$)$_3$ when

L is PMe$_2$Ph and PMePh$_2$,[3] whereas the mononuclear species *cis*-[L$_2$Pt{9-MeAd(-H)-N^6N^7}]NO$_3$ is formed when L is PPh$_3$.[4] Similarly, deprotonation of 1-methylcytosine (1-MeCy) leads to the polynuclear adducts *cis*-[L$_2$Pt{1-MeCy-(-H)-N^3N^4}]$_3$(NO$_3$)$_3$ with the less hindered phosphines PMe$_3$[5] and PMe$_2$Ph,[6] while the mononuclear species *cis*-[L$_2$Pt{1-MeCy(-H)-N^4}(1-MeCy-N^3)](NO$_3$) is quantitatively obtained when L is PPh$_3$.[6]

In this paper, we report the synthesis and characterization of the complexes *cis*-[(PPh$_3$)$_2$Pt(nucleobase)(ONO$_2$)]NO$_3$ and *cis*-[(PPh$_3$)$_2$Pt(nucleobase)$_2$](NO$_3$)$_2$, containing the neutral nucleobases 1-MeCy and 9-methylguanine (9-MeGu) acting as monodentate ligands. Early studies have shown that the nitrato complexes *cis*-L$_2$Pt(ONO$_2$)$_2$, obtained from the cis-

(1) Lippert, B.; Müller, J. *Concepts and Models in Bioinorganic Chemistry*; Kraatz, H.-B., Metzler-Nolte, N., Eds.; Wileys-VCH: Weinheim, Germany, 2006; p 137.

(2) Schenetti, L.; Mucci, A.; Longato, B. *J. Chem. Soc., Dalton Trans.* **1996**, 299.

(3) (a) Longato, B.; Pasquato, L.; Mucci, A.; Schenetti, L. *Eur. J. Inorg. Chem.* **2003**, 128. (b) Longato, B.; Pasquato, L.; Mucci, A.; Schenetti, L.; Zangrando, E. *Inorg. Chem.* **2003**, *42*, 7861.

(4) Montagner, D.; Longato, B. *Inorg. Chim. Acta*, **2007**, doi: 10.1016/j.ica.2007.02.025.

(5) Trovò, G.; Bandoli, G.; Casellato, U.; Corain, B.; Nicolini, M.; Longato, B. *Inorg. Chem.* **1990**, *29*, 4616.

(6) Longato, B.; Montagner, D.; Zangrando, E. *Inorg. Chem.* **2006**, *45*, 8179.

platin analogues *cis*-L$_2$PtCl$_2$ (L = tertiary phosphines), in reactions with 1 equiv of these nucleobases, form mixtures of *cis*-[L$_2$Pt(nucleobase)]$^{2+}$ and *cis*-[L$_2$Pt(nucleobase)$_2$]$^{2+}$, in equilibrium with the unreacted starting nitrate. The relatively high stability of the bisadducts precludes the isolation of the intermediate species *cis*-[L$_2$Pt(nucleobase)]$^{2+}$.[3] However, the presence of PPh$_3$ ligands stabilizes enough such intermediates to allow their isolation as pure compounds. The single-crystal X-ray analyses of *cis*-[(PPh$_3$)$_2$Pt(1-MeCy)(ONO$_2$)]$^+$ and *cis*-[(PPh$_3$)$_2$Pt(9-MeGu)(ONO$_2$)]$^+$ are reported here along with a study of their behavior in solution by NMR spectroscopy. With the less hindered phosphine PMePh$_2$, we were able to isolate only the bisadducts *cis*-[(PMePh$_2$)$_2$Pt(1-MeCy)$_2$]$^{2+}$ and *cis*-[(PMePh$_2$)$_2$Pt(1-MeCy)$_2$]$^{2+}$, whose X-ray structures are also described. Finally, the relative stabilities of the monoadducts *cis*-[L$_2$Pt(nucleobase)]$^{2+}$ (L = PMePh$_2$, PPh$_3$) have been evaluated.

Experimental Section

Instrumentation and Materials. NMR spectra of various solvents at 300 K were obtained in solution in 5-mm sample tubes for ^{1}H, ^{31}P, and ^{195}Pt (operating at 300.13, 121.5, and 64.2 MHz, respectively) with a Bruker AVANCE 300 MHz spectrometer equipped with a variable-temperature apparatus and for ^{15}N (operating at 40.6 MHz) with a Bruker 400 AMX-WB spectrometer. The ^{1}H NMR chemical shifts were referenced to the residual impurity of the solvent. The external references were H$_3$PO$_4$ (85% w/w in D$_2$O) for ^{31}P, Na$_2$PtCl$_4$ in D$_2$O (adjusted to $\delta = -1628$ ppm from Na$_2$PtCl$_6$) for ^{195}Pt, and CH$_3$NO$_2$ (in CDCl$_3$ at 50% w/w) for ^{15}N. Inverse-detected spectra were obtained through hetero-nuclear multiple-bond (HMBC) correlation experiments, using parameters similar to those previously reported.[2]

The solvents CDCl$_3$, DMSO-d_6, DMF-d_7, and CD$_2$Cl$_2$ and the reagent 9-MeGu (Aldrich) were used as received unless otherwise stated. *cis*-(PPh$_3$)$_2$PtCl$_2$,[7] *cis*-(PMePh$_2$)$_2$Pt(ONO$_2$)$_2$ (**1b**),[3] *cis*-(PMe$_3$)$_2$Pt(NO$_3$)$_2$,[5] and 1-MeCy[8] were synthetized as previously reported. *cis*-(PPh$_3$)$_2$Pt(ONO$_2$)$_2$ (**1a**), recently described by us,[4] crystallized from dimethylformamide (DMF) in the presence of diethyl ether vapors, gave crystals having the composition **1a**·DMF, as shown by ^{1}H NMR and elemental analysis. Elem anal. Calcd for C$_{39}$H$_{37}$N$_3$O$_7$P$_2$Pt: C, 51.09; H, 4.07; N, 4.58. Found: C, 51.21; H, 3.93; N, 4.27. A CHCl$_3$ solution of **1a**, allowed to concentrate at room temperature, released crystals appropriate for X-ray analysis, having the composition *cis*-(PPh$_3$)$_2$Pt(ONO$_2$)$_2$·CHCl$_3$.

Preparation of the Complexes. Synthesis of *cis*-[(PPh$_3$)$_2$Pt-(1-MeCy)(ONO$_2$)](NO$_3$) (2a). To a solution of **1a**·DMF (73.4 mg, 0.08 mmol) in DMF (3 mL) was added 10.2 mg of 1-MeCy (0.08 mmol), under stirring at room temperature, obtaining a solution in ca. 10 min. The addition of Et$_2$O (10 mL) afforded a white precipitate, which was recovered by filtration and dried under vacuum. The yield of a solid, having the composition *cis*-(PPh$_3$)$_2$Pt(1-MeCy)(NO$_3$)$_2$·DMF, was 55 mg (66%). Elem anal. Calcd for C$_{44}$H$_{44}$N$_6$O$_8$P$_2$Pt: C, 50.72; H, 4.26; N, 8.07. Found: C, 49.76; H, 4.14; N: 8.08. ^{1}H NMR in DMSO-d_6 (δ): 8.72 (br s, 1H, NH$_2$), 8.08 (br s, 1H, NH$_2$), 7.60–7.35 (c m, 31H, PPh$_3$ and H6), 5.60 and 5.45 [d, $^3J_{HH}$ = 7.1 Hz H5], 2.91 and 3.08 (s, 3H, NCH$_3$). DMF resonances: 7.94 (s, 1H, CHO), 2.88 (s, 3H, CH$_3$), 2.72 (s, 3H, CH$_3$). ^{31}P{^{1}H} NMR in DMSO-d_6 (δ): two AB multiplets at

5.36 (d, $^2J_{PP}$ = 22.6 Hz, $^1J_{PPt}$ = 4080 Hz), 5.12 (d, $^2J_{PP}$ = 22.6 Hz, $^1J_{PPt}$ = 3536 Hz), 4.60 (d, $^2J_{PP}$ = 21.4 Hz), 4.02 (d, $^2J_{PP}$ = 21.4 Hz) with relative intensities 9:1, respectively. ^{31}P{^{1}H} NMR in DMF (δ): two AB multiplets at 5.07 (d, $^2J_{PP}$ = 22.3 Hz, $^1J_{PPt}$ = 4015 Hz), 4.51 (d, $^2J_{PP}$ = 22.3 Hz, $^1J_{PPt}$ = 3488 Hz), 5.02 (d, $^2J_{PP}$ = 21.4 , $^1J_{PPt}$ = 4015 Hz), 4.48 (d, $^2J_{PP}$ = 21.4 Hz, $^1J_{PPt}$ = 3488 Hz) with relative intensities 1:1, respectively. The same synthesis, carried out in CH$_2$Cl$_2$, followed by precipitation with Et$_2$O affords **2a**, with a yield of 70%. ^{1}H NMR in CD$_2$Cl$_2$ (δ): 9.47 (br s, 1H, NH$_2$), 7.71–7.28 (c m, 30H, PPh$_3$), 7.12 (br s, 1H, NH$_2$), 6.81 (d, $^3J_{HH}$ = 7.0 Hz, 1H, H6], 5.85 [d, $^3J_{HH}$ = 7.0 Hz, 1H, H5], 3.20 (s, 3H, NCH$_3$). ^{31}P{^{1}H} NMR in CD$_2$Cl$_2$ (δ): AB multiplet at 5.11 (d, $^2J_{PP}$ = 21.3 Hz, $^1J_{PPt}$ = 3939 Hz), 3.58 (d, $^2J_{PP}$ = 21.3 Hz, $^1J_{PPt}$ = 3455 Hz). ^{195}Pt NMR (δ) in CH$_2$Cl$_2$: −4163 (dd, $^1J_{PPt}$ = 3430 and 3960 Hz). Crystals for X-ray analysis, having the composition **2a**·3DMF, were obtained from a DMF solution of **2a** by slow diffusion of diethyl ether vapors, at room temperature.

Synthesis of *cis*-[(PPh$_3$)$_2$Pt(9-MeGu)(ONO$_2$)](NO$_3$)·2DMF (3a). By using the procedure of **2a**, complex **3a** was isolated with a yield of 55%. Diffusion of Et$_2$O into a DMF solution afforded colorless crystals having the composition *cis*-(PPh$_3$)$_2$Pt(9-MeGu)-(NO$_3$)$_2$·2DMF. Elem anal. Calcd for C$_{42}$H$_{37}$N$_8$O$_8$P$_2$Pt: C, 48.56; H, 3.60; N, 10.78. Found: C, 48.91; H, 3.72; N, 10.31. ^{1}H NMR in DMSO-d_6 (δ): 11.5 (br s, 1H, N1H), 8.66 (s, 1H, H8), 7.6–7.3 (c m, 30H, PPh$_3$), 6.95 (br s, 2H, NH$_2$), 3.38 (s, 3H, NCH$_3$). DMF resonances: 7.94 (s, 1H, CHO), 2.88 (s, 3H, CH$_3$), 2.72 (s, 3H, CH$_3$). ^{31}P{^{1}H} NMR in DMSO-d_6 (δ): AB multiplets at 7.94 (d, $^2J_{PP}$ = 22.6 Hz, $^1J_{PPt}$ = 3482 Hz), 5.12 (d, $^2J_{PP}$ = 22.6 Hz, $^1J_{PPt}$ = 4048 Hz). ^{31}P{^{1}H} NMR in DMF (δ): two AB multiplets at 7.12 (d, $^2J_{PP}$ = 22.6 Hz, $^1J_{PPt}$ = 3465 Hz), 4.99 (d, $^2J_{PP}$ = 22.6 Hz, $^1J_{PPt}$ = 4032 Hz), 5.71 (d, $^2J_{PP}$ = 22.6 Hz, $^1J_{PPt}$ = 3465 Hz), 4.92 (d, $^2J_{PP}$ = 22.6 Hz, $^1J_{PPt}$ = 4032 Hz). There were minor resonances at 5.73 and 5.46 ppm (apparent singlets). **3a** is insoluble in chlorinated solvents. Crystals for X-ray analysis, having the composition **3a**·2DMF, were obtained from a DMF solution of **3a** by slow diffusion of diethyl ether vapors, at room temperature.

Synthesis of *cis*-[(PPh$_3$)$_2$Pt(1-MeCy)$_2$](NO$_3$)$_2$ (4a). To a solution of *cis*-[(PPh$_3$)$_2$Pt(NO$_3$)$_2$]·DMF (35.3 mg, 0.04 mmol) in CH$_2$Cl$_2$ (2.5 mL) was added 9.8 mg of 1-MeCy (0.08 mmol), and the suspension was stirred at room temperature for 17 h. The resulting solid was recovered by filtration, washed with pentane, and dried under vacuum. The product was purified by dissolution in DMF and precipitated with Et$_2$O. The yield of **4a** was 28.9 mg (68%). Elem anal. Calcd for C$_{46}$H$_{44}$N$_8$O$_8$P$_2$Pt: C, 50.50; H, 4.05; N, 10.24. Found: C, 50.56; H, 4.48; N, 10.49. ^{1}H NMR in DMSO-d_6 (δ): 9.04 (br s, 1H, NH$_2$), 7.93 (br s, 1H, NH$_2$), 7.6–7.3 (c m, 16H, PPh$_3$ and H6), 5.78 (d, $^3J_{HH}$ = 7.3 Hz, 1H, H5), 2.91 (s, 3H, NCH$_3$). ^{31}P{^{1}H} NMR in DMSO-d_6 (δ): −0.81 (s, $^1J_{PPt}$ = 3525 Hz). ^{195}Pt NMR in CH$_2$Cl$_2$ (δ): −4198 (s, $^1J_{PPt}$ = 3540 Hz).

Synthesis of *cis*-[(PMePh$_2$)$_2$Pt(1-MeCy)$_2$](NO$_3$)$_2$ (4b). A solution of *cis*-(PMePh$_2$)$_2$Pt(ONO$_2$)$_2$ (80.8 mg, 0.11 mmol) and 28 mg of 1-MeCy (0.22 mmol) in DMF (4 mL) was stirred at room temperature for 1 h. The addition of Et$_2$O (25 mL) afforded a powdered solid, which was recovered by filtration, washed with ether, and dried under vacuum. The product was purified by dissolution in DMF and precipitated with Et$_2$O. The yield of *cis*-[(PMePh$_2$)$_2$Pt(1-MeCy)$_2$](NO$_3$)$_2$ was 69 mg (65%). Elem anal. Calcd for C$_{36}$H$_{40}$N$_8$O$_8$P$_2$Pt: C, 44.59; H, 4.17; N, 11.55. Found: C, 44.34; H, 4.48; N, 11.80. ^{1}H NMR in DMSO-d_6 (δ): 8.88 (br s, 1 H, NH$_2$), 7.97 (br s, 1 H, NH$_2$), 7.6–7.3 (c m, 10H, PMe*Ph$_2$*), 7.35 (d, $^3J_{HH}$ = 7.2 Hz, 1H, H6), 5.55 (d, $^3J_{HH}$ = 7.1 Hz, 1H, H5), 3.06 (s, 3H, NCH$_3$), 1.89 (d, $^2J_{HP}$ = 9.2 Hz, 3H, PMe*Ph$_2$*). ^{31}P{^{1}H} NMR in

(7) Chock, P. B.; Halpern, J.; Paulick, F. E. *Inorg. Synth.* **1973**, *14*, 90.
(8) Kistenmacher, T. J.; Rossi, M.; Caradonna, J. P.; Marzilli, L. G. *Adv. Mol. Relax. Interact. Processes* **1979**, *15*, 119.

Table 1. Crystallographic Data and Details of Structure Refinements for Compounds **1a**–**3a**, **4b**, and **5b**

	1a·CHCl$_3$	**2a**·3DMF	**3a**·2DMF	**4b**·2DMF	**5b**·4DMF
formula	C$_{37}$H$_{31}$Cl$_3$N$_2$O$_6$P$_2$Pt	C$_{50}$H$_{58}$N$_8$O$_{10}$P$_2$Pt	C$_{48}$H$_{51}$N$_9$O$_9$P$_2$Pt	C$_{42}$H$_{54}$N$_{10}$O$_{10}$P$_2$Pt	C$_{50}$H$_{68}$N$_{16}$O$_{12}$P$_2$Pt
M_r	963.02	1188.07	1155.01	1115.98	1342.23
cryst syst	monoclinic	triclinic	monoclinic	monoclinic	triclinic
space group	$P2_1/n$	$P\bar{1}$	$P\,2_1/n$	$P2_1/n$	$P\bar{1}$
a (Å)	12.043(3)	10.809(3)	15.046(3)	10.501(2)	11.754(3)
b (Å)	20.007(3)	13.033(3)	22.337(3)	25.022(3)	15.387(3)
c (Å)	15.846(3)	19.209(4)	17.389(3)	17.850(3)	18.652(4)
α (deg)		87.99(2)			68.05(3)
β (deg)	95.35(2)	74.77(2)	112.17(2)	97.81(2)	76.46(3)
γ (deg)		88.41(2)			76.54(3)
V (Å^3)	3801.4(13)	2608.9(11)	5412.1(16)	4646.7(13)	3002.2(12)
Z	4	2	4	4	2
D_{calcd} (g cm^{-3})	1.683	1.512	1.418	1.595	1.485
Mo Kα (mm^{-1})	4.034	2.814	2.710	4.743	2.461
$F(000)$	1896	1198	2328	2256	1368
θ range (deg)	1.98–31.08	2.48–30.61	2.34–25.68	5.52–31.75	2.00–26.37
reflns collected	53 841	37 778	64 637	26 946	34 058
unique reflns	10 800	14 664	10 062	5260	9970
R_{int}	0.0449	0.0337	0.0883	0.0430	0.0771
obsd $I > 2\sigma(I)$	7449	12 450	4519	4993	4942
refined param	460	660	613	563	734
GOF (F^2)	0.898	0.963	0.819	1.157	0.834
R1 [$I > 2\sigma(I)$]^a	0.0313	0.0315	0.0443	0.0495	0.0539
wR2^a	0.0713	0.0798	0.0966	0.1114	0.1087
residuals (e Å^{-3})	0.674, –0.613	0.602, –0.842	0.739, –0.832	1.153,^{b} –0.878	1.798,^{c} –1.074

^{a} R1 = $\sum||F_o| - |F_c||/\sum|F_o|$, wR2 = $[\sum w\,(F_o{}^2 - F_c{}^2)^2/\sum w\,(F_o{}^2)^2]^{1/2}$. ^{b} Residual located near a lattice DMF molecule. ^{c} Residual located at 1.1 Å from the metal ion.

DMSO-d_6 (δ): −11.13 (s, $^1J_{PPt}$ = 3322 Hz). Crystals for X-ray analysis, analyzed as **4b**·2DMF (by NMR), were obtained by slow diffusion of Et$_2$O vapors into a DMF solution of **4b**.

Synthesis of *cis*-[(PPh$_3$)$_2$Pt(9-MeGu)$_2$](NO$_3$)$_2$ (5a). To a solution of *cis*-[(PPh$_3$)$_2$Pt(ONO$_2$)$_2$]·DMF (50.9 mg, 0.06 mmol) in 3 mL of CH$_2$Cl$_2$was added 18.6 mg of 9-MeGu (0.12 mmol), and the suspension was stirred at room temperature for 36 h. The resulting white solid was recovered by filtration, washed with CH$_2$Cl$_2$, and dried under vacuum. The sample was purified from DMF/Et$_2$O. The yield of **5a** was 55 mg (84%). Elem anal. Calcd for C$_{48}$H$_{44}$N$_{10}$O$_8$P$_2$Pt: C, 49.10; H, 3.78; N, 14.32. Found: C, 48.73; H, 3.71; N, 14.29. ^{1}H NMR in DMSO-d_6 (δ): 11.3 (br s, 1H, N1H), 7.74 (s, 1H, H8), 7.6–7.3 (c m, 15H, PPh$_3$), 6.81 (br s, 2H, NH$_2$), 3.27 (s, 3H, NCH$_3$). ^{31}P{^{1}H} NMR in DMSO-d_6 (δ): 1.54 (s, $^1J_{PPt}$ = 3507 Hz). ^{15}N NMR (inverse detected) in DMSO-d_6 (δ): −203 (N7), −216 (N9), −226 (N1H), –297 (N2H$_2$).

Synthesis of *cis*-[(PMePh$_2$)$_2$Pt(9-MeGu)$_2$](NO$_3$)$_2$ (5b). With the procedure reported for **5a**, **5b** was prepared with a yield of 67% from **1b** (102 mg, 0.14 mmol) and 9-MeGu (46 mg, 0.28 mmol) in CH$_2$Cl$_2$ (10 mL). Elem anal. Calcd for C$_{38}$H$_{40}$N$_{12}$O$_8$P$_2$Pt: C, 43.48; H, 3.85; N, 16.00. Found: C, 43.52; H, 4.46; N, 15.97. ^{1}H NMR in DMSO-d_6 (δ): 11.16 (br s, 1H, N1H), 7.87 (s, 1H, H8), 7.7–7.1 (c m, 10H, PMe*Ph$_2$*), 6.84 (br s, 2H, NH$_2$), 3.28 (s, 3H, NCH$_3$), 1.93 (d, $^2J_{HP}$ = 8.7 Hz, 3H, P*Me*Ph$_2$). ^{31}P{^{1}H} NMR in DMSO-d_6 (δ): −9.21 (s, $^1J_{PPt}$ = 3341 Hz). ^{15}N NMR (inverse detected) in DMSO-d_6 (δ): −198 (N7), −216 (N9), −227 (N1H), –297 (N2H$_2$). Crystals for X-ray analysis were obtained by slow diffusion of Et$_2$O vapors into a DMF solution of **5b**.

X-ray Structure Determinations. Crystal data and details of structural refinements are reported in Table 1.

Diffraction data for compounds **1a**–**3a** and **5b** were collected on a Nonius DIP-1030H system equipped with Mo Kα radiation ($\lambda = 0.710\,73$ Å) at ambient temperature, except the data collection of **2a**, which was performed at $T = 200(2)$ K. Because of the small crystal dimensions (approximately $0.15 \times 0.14 \times 0.10$ mm), the intensity data of **4b** were measured at the RX diffraction beamline of Elettra Synchrotron, Trieste, Italy [CCD MarResearch detector,

$\lambda = 1.000\,00$ Å, $T = 100(2)$ K]. Cell refinement, indexing, and scaling of all of the data sets were carried out using *Denzo*[9] and *Scalepack*.[9] All of the structures were solved by direct methods and subsequent difference Fourier analyses[10] and refined by the full-matrix least-squares method based on F^2 with all observed reflections.[10] Besides the nitrate anions, the difference Fourier maps revealed that some solvent residuals successfully interpreted as chloroform in **1a** and dimethylformamide in **2a**, **3a**, **4b**, and **5b**, accounting for three, two, two, and four molecules for metal units, respectively; some of these were found to be disordered over two positions. All hydrogen atoms were located at geometrical positions, except those of disordered solvent molecules; those of cytosine exocyclic amino groups in **2a** and **5a** were derived from the difference Fourier map. The crystal packing of both compounds evidence about 30% of the unit cell accessible to the solvent, and three lattice DMF molecules per complex unit in **2a** (two in **3a**) were detected on the difference Fourier map and successfully refined. The volume left out in the crystal by the complexes and nitrate anions accounts for about 22 and 38% of the unit cell in **4b** and **5b**, and two and four solvent DMF molecules (per complex unit), respectively, occupy this area. All of the calculations were performed using the WinGX system, version 1.70.05.[11]

Results and Discussion

1. Structural Characterization of 1a. The removal of the chloride ligands in *cis*-[(PPh$_3$)$_2$PtCl$_2$], using AgNO$_3$, leads to the dinitrato complex **1a** and its crystallization in DMF, in the presence of diethyl ether vapors, or in CHCl$_3$ affords crystals having the composition **1a**·DMF or **1a**·CHCl$_3$,

(9) Otwinowski, Z.; Minor, W. Processing of X-ray Diffraction Data Collected in Oscillation Mode. In *Methods in Enzymology*; Carter, C. W., Jr., Sweet, R. M., Eds.; Academic Press: New York, 1997; Vol. *276*, p 307.
(10) Sheldrick, G. M. *SHELX97, Programs for Crystal Structure Analysis*, release 97-2; University of Göttingen: Göttingen, Germany, 1998.
(11) Farrugia, L. J. *J. Appl. Crystallogr.* **1999**, *32*, 837.
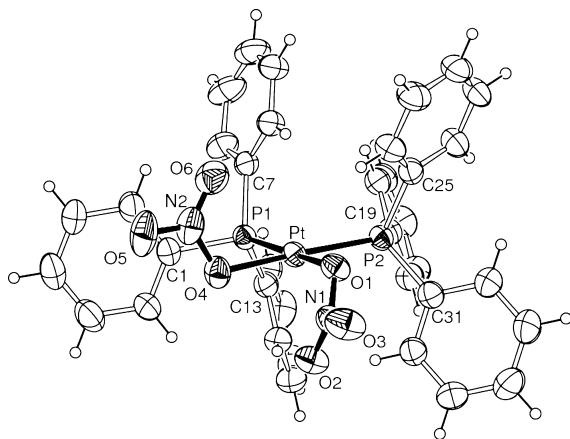
Figure 1. ORTEP drawing of complex **1a** (only *ipso*-carbon atoms are labeled for clarity). Selected bond lengths (Å) and angles (deg): Pt–O1 2.093(2), Pt–O4 2.105(3), Pt–P1 2.239(1), Pt–P2 2.248(1); O1–Pt–O4 84.70(10), O1–Pt–P1 174.61(7), O4–Pt–P1 90.89(8), O1–Pt–P2 87.44(8), O4–Pt–P2 172.14(7), P1–Pt–P2 96.97(4), N1–O1–Pt1 113.8(6), N2–O4–Pt1 115.6(7).

Figure 2. $^{31}P\{^1H\}$ NMR spectra (0.1 M) of **1a** in (a) $CDCl_3$, (b) DMSO-d_6, (c) DMF-d_7 (25 °C), and (d) DMF-d_7 (−60 °C) and (e) an expansion of part d.

respectively. The X-ray structure of **1a**·CHCl₃ reveals one independent complex cocrystallized with a molecule of chloroform.

Figure 1 reports the ORTEP drawing of the metal complex. The platinum displays a distorted square coordination, bound to the P donors and O nitrate atoms, in a cis configuration. The nitrato groups are directed on opposite sides with respect to the coordination plane, and their mean planes form dihedral angles of 69.1(1) and 84.9(1)° with it. No significant displacement of the metal from the P_2O_2 plane is detected, and the donor atoms are coplanar within ±0.03 Å. Phenyl rings C13 and C19 are involved in $\pi-\pi$ stacking interaction [centroid-to-centroid distance of 3.644(2) Å], but no intermolecular phenyl interaction is detected in the crystal. The coordination bond lengths and angles, as well as the orientation of nitrate anions, are very similar to those detected in the $PMePh_2$,[3] PMe_3,[12] and PEt_3[13] derivatives. This last feature, however, contrasts with that found in the analogue *cis*-$(NH_3)_2Pt(ONO_2)_2$, in which the nitrate groups lie on the same side of the ligand plane.[14]

In a solution of coordinating solvents, **1a** undergoes an extensive solvolysis of the Pt–O bonds, with the formation of complexes in which one or both of the NO_3^- ligands are replaced by solvent molecules. The process is clearly evidenced by ^{31}P NMR spectroscopy, as is illustrated in Figure 2.

In $CDCl_3$ at 27 °C (Figure 2a), the $^{31}P\{^1H\}$ NMR spectrum of **1a** exhibits a sharp singlet at δ 3.35 ppm flanked by ^{195}Pt NMR satellites ($^1J_{PPt}$ = 4018 Hz), while in DMSO-d_6 (Figure 2b), the signal is broad and shifted at lower field (δ 4.6 ppm, with $^1J_{PPt}$ = ca. 4070 Hz), indicative of chemical exchange between the NO_3^- ligands and the solvent molecules. Figure 2c shows the spectrum of a freshly prepared solution of **1a** in DMF-d_7 (ca. 0.1 M), characterized by two broad reso-
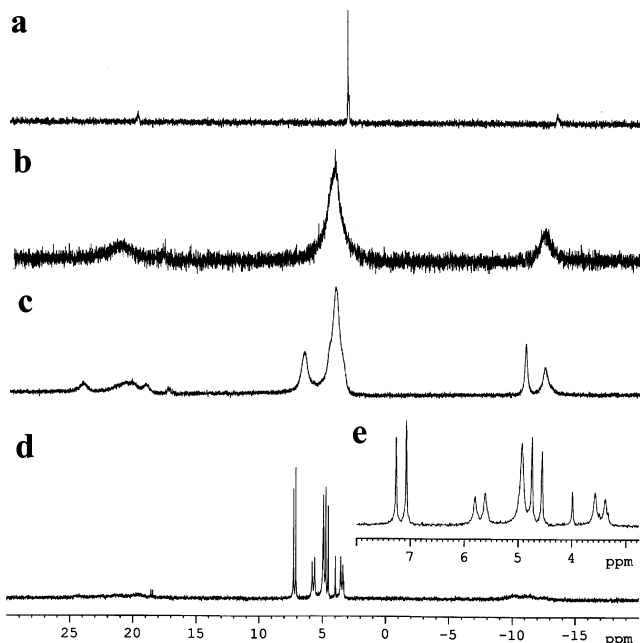
nances (at δ 6.68 and 4.28 ppm, with $^1J_{PPt}$ values in the range 4050–4260 Hz), which does not change after some hours at room temperature. When the solution is cooled at −60 °C (Figure 2d), the spectrum shows two AB multiplets, one sharp (at δ 7.15 and 4.7 ppm, $^2J_{PP}$ = 22.9 Hz, relative intensity 39%) and the second (at δ 5.7 and 3.5 ppm, $^2J_{PP}$ = 23.3 Hz) less intense (27%) and broader. Both of them are consistent with the presence of monosubstituted species of the type *cis*-$[(PPh_3)_2Pt(ONO_2)(DMF)]^+$, in which the NO_3^- group behaves as a monodentate ligand, and/or as a bridging ligand, in polynuclear species. The remaining resonances (Figure 2e) at δ 4.93 (slightly broad singlet, relative intensity 26%) and δ 3.99 ppm (singlet, relative intensity 8%) are tentatively attributed to the species *cis*-$[(PPh_3)_2Pt(DMF)_2]^{2+}$ and unsolvated species *cis*-$(PPh_3)_2Pt(ONO_2)_2$. The absence of resolved ^{195}Pt satellites (at −60 °C) precludes a deeper insight into the nature of species in equilibrium.

2. X-ray Structures of *cis*-$[(PPh_3)_2Pt(nucleobase)$-$(ONO_2)]^+$ (nucleobase = 1-MeCy, 2a; 9-MeGu, 3a) and *cis*-$[(PMePh_2)_2Pt(nucleobase)_2]^{2+}$ (nucleobase = 1-MeCy, 4b; 9-MeGu, 5b). The addition of 1 equiv of 1-MeCy to a DMF solution of **1a**, followed by condensation of diethyl ether vapors, afforded crystals having the composition **2a**·3DMF, as established by ^1H NMR and X-ray structure determination. Similarly, with 9-MeGu the analogue complex **3a**·2DMF has been isolated in good yield. In the presence of 2 equiv of nucleobase, the bisadducts **4a** and **5a** are formed in quantitative yield (by NMR).

The monoadduct complexes **2a** and **3a**, reported in Figures 3 and 4, present close similarities not only in the conformation but also in the crystal packing and will be discussed together.

The Pt ion exhibits a square-planar coordination sphere achieved through the phosphorus atoms, the nitrogen donor from the nucleobase, and the nitrate oxygen atom. The

(12) Suzuki, Y.; Miyamoto, T. K.; Ichida, H. *Acta Crystallogr., Sect. C* **1993**, *49*, 1318.

(13) Kuehl, C. J.; Tabellion, F. M.; Arif, A. M.; Stang, P. J. *Organometallics* **2001**, *20*, 1956.

(14) Lippert, B.; Lock, C. J. L.; Rosemberg, B.; Zvagulis, M. *Inorg. Chem.* **1977**, *16*, 1525.
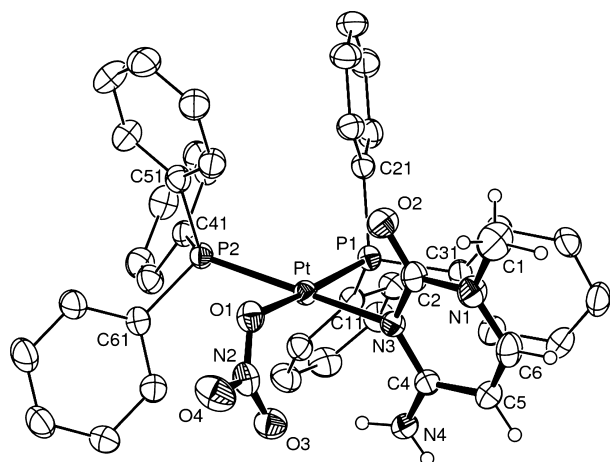
Figure 3. ORTEP drawing (35% probability ellipsoid) of the complex cation of **2a**. Only *ipso*-carbon atoms are labeled for the sake of clarity.
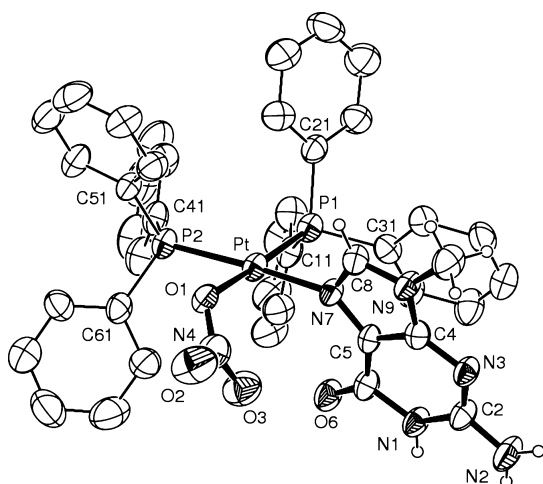

Figure 4. ORTEP drawing (35% probability ellipsoid) of the complex cation of **3a**. Only *ipso*-carbon atoms are labeled for the sake of clarity.

nucleobase is bound to the metal through N3 of 1-MeCy and N7 of 9-MeGu, which represent the preferential binding sites for pyrimidine and purine bases, respectively. The bond distances and angles are reported in Table 2 and do not show any anomaly. The Pt−N3 bond distance in **2a** [2.101(2) Å] is slightly longer than the corresponding distance Pt−N7 in **3a** [2.075(5) Å] and can be ascribed to the endocyclic C−N_d−C angle (N_d being the donor site), narrower in the five-membered ring than in the six-membered ring, which allows a closer approach of the ligand to the metal center.

Both of the bases have an unsymmetrical coordination; in fact, the C2−N3−Pt angle of the cytosine (on the side of the exocyclic amino group) and the C5−N7−Pt one of the guanine (carbonyl group side) are larger by ca. 12° and ca. 7° than the C4−N3−Pt and C8−N7−Pt angles, respectively. As far as Pt−P bond lengths are concerned, it is worth noting the shorter value measured for the phosphine trans to the nitrate anion, and the narrower N−Pt−O1 angle [86.39(10) and 86.9(2)°] in **2a** and **3a**, respectively] in comparison to the P1−Pt−P2 one [98.83(3) and 98.08(7)°], likely induced by steric requirements.

The 1-MeCy and 9-MeGu bases are oriented almost normal to the coordination mean plane, forming a close comparable angle with the latter of ca. 76° in both complexes.

Table 2. Coordination Bond Lengths (Å) and Angles (deg) and Geometrical Parameters for **2a** and **3a**

	2a	3a
Pt−N3/7[a]	2.100(2)	2.075(5)
Pt−O1	2.117(2)	2.140(5)
Pt−P1	2.2508(9)	2.247(2)
Pt−P2	2.2846(9)	2.2780(18)
N3/7−Pt−O1	86.37(10)	86.9(2)
N3/7−Pt−P1	90.81(7)	90.38(17)
N3/7−Pt−P2	169.08(7)	171.40(17)
O1−Pt−P1	173.61(7)	173.88(15)
O1−Pt−P2	83.53(7)	84.51(13)
P1−Pt−P2	98.82(3)	98.08(7)
N2−O1−Pt	116.37(18)	
C2−N3−Pt	112.92(19)	
C4−N3−Pt	124.9(2)	
N4−O1−Pt		117.9(5)
C5−N7−Pt		130.0(5)
C8−N7−Pt		123.0(5)
base/coord plane NOP₂ (deg)	76.38(8)	76.91(9)
NO₃/coord plane NOP₂ (deg)	68.3(1)	61.7(2)

[a] N3 refers to **2a** and N7 to **3a**.

On the other hand, the nitrate group is more bent, and the mean plane figures out a dihedral angle of 65° (mean value for the two structures), with nitrate oxygen O3 pointing toward the cytosine exocyclic amino group N4 in **2a** (at a hydrogen-bond distance from the latter, O3−N4 = 2.99 Å) and toward the guanine carboxyl oxygen in **3a** (O3−O6 = 3.09 Å). In both complexes, the phosphine phenyl group C31 is oriented in such a way as to favor an intramolecular $\pi-\pi$ interaction with the model nucleobase (centroid-to-centroid distance of ca. 3.5 Å). Moreover, an intramolecular stacking interaction is detected in **3a** between phenyl rings C11 with C41 [distance between centroids = 3.587(7) Å]. The corresponding distance in **2a** is slightly longer [4.007(2) Å], indicating a different, although small, difference in the conformations of the phosphine ligands.

Whereas we were unable to grow crystals of **4a** and **5a** for X-ray analyses, this was possible for the PMePh₂ analogues, **4b** and **5b**, easily prepared from **1b** in the presence of 2 equiv of 1-MeCy and 9-MeGu, respectively. The X-ray structural analysis of **4b** and **5b** confirms the formation of the bisadducts species *cis*-[(PMePh₂)₂Pt(1-MeCy)₂]²⁺ and *cis*-[(PMePh₂)₂Pt(9-MeGu)₂]²⁺, and an ORTEP view of these complexes, showing similar geometrical features, are illustrated in Figures 5 and 6, while the structural data are collected in Table 3.

The bases, bound through N3 and N7 in **4b** and **5b**, respectively, assume a head-to-tail arrangement that is the most frequent orientation of two bases in a square-planar geometry.[15] The Pt−N and Pt−P coordination bond lengths follow a trend as observed in the monoadduct complexes. The C4−N3−Pt and C8−N7−Pt angles in **4b** and **5b** are significantly larger than the C2−N3−Pt and C5−N7−Pt ones, respectively, confirming an unsymmetrical coordination of the bases (Table 3). Coordination Pt−N distances compare well with those found in the correspondent PMe₃ deriva-

(15) Zangrando, E.; Pichierri, F.; Randaccio, L.; Lippert, B. *Coord. Chem. Rev.* **1996**, *156*, 275.
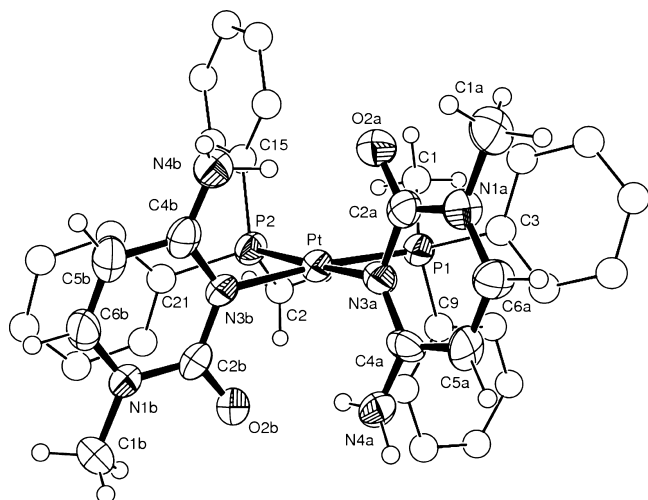
Figure 5. ORTEP drawing (35% probability ellipsoid) of the complex cation of **4b**. Phosphine carbon atoms as spheres of the fixed radius are labeled for the sake of clarity.
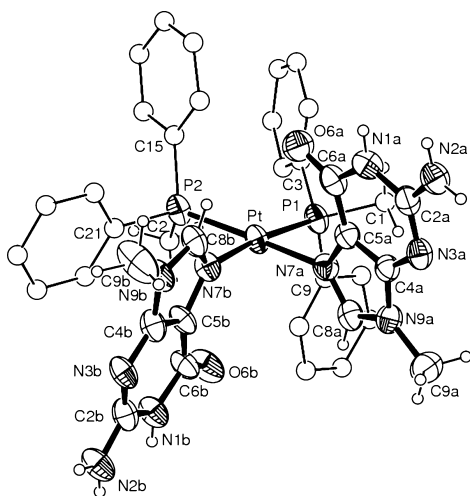

Figure 6. ORTEP drawing (35% probability ellipsoid) of the complex cation of **5b**.

tives,[16,17] although the structural characterization of the *cis*-[(PMe₃)₂Pt(9-MeGu)₂]²⁺ species[17] is less accurate. The Pt—P bond distances appear only slightly longer in the present complexes containing the bulkier PMePh₂ (2.270 and 2.262 Å mean values in **4b** and **5b**, respectively) when compared with the average values of 2.255 and 2.250 Å of the PMe₃ complexes.

The complex **4b** presents a pseudo-2-fold symmetry in the solid state for the conformation assumed by the PMePh₂ ligands (methyl groups on different sides of the coordination plane) and a head-to-tail arrangement of the bases. This allows the formation of intermolecular hydrogen bonds between each exocyclic NH₂ group and the carbonyl of the adjacent base (N4···O2 distances of 2.87 and 2.94 Å). The other NH₂ hydrogen atom of each cytosine forms a hydrogen bond with a nitrate anion (N4—H···O of 2.85 Å, mean distance). Intramolecular π—π interactions occur between

(16) Trovò, G.; Valle, G.; Longato, B. *J. Chem. Soc., Dalton Trans.* **1993**, 669.
(17) Longato, B.; Bandoli, G.; Trovò, G.; Marasciulo, E.; Valle, G. *Inorg. Chem.* **1995**, *34*, 1745.

Table 3. Coordination Bond Lengths (Å) and Angles (deg) and Geometrical Parameters for **4b** and **5b**

	4b	5b
Pt—N3a/7a[a]	2.106(7)	2.087(7)
Pt—N3b/7b	2.095(8)	2.082(7)
Pt—P1	2.265(2)	2.268(3)
Pt—P2	2.275(2)	2.256(3)
N3a—Pt—N3b	86.3(3)	
N7a—Pt—N7b		84.7(3)
N3a/7a—Pt—P1	89.5(2)	89.2(2)
N3b/7b—Pt—P1	174.3(2)	172.9(2)
N3a/7a—Pt—P2	176.1(2)	174.7(2)
N3b/7b—Pt—P2	91.5(2)	90.2(2)
P1—Pt—P2	92.88(9)	95.91(9)
C2a—N3a—Pt	113.4(6)	
C4a—N3a—Pt	125.2(6)	
C2b—N3b—Pt	114.4(7)	
C4b—N3b—Pt	123.1(6)	
C5a—N7a—Pt		121.5(6)
C8a—N7a—Pt		131.1(6)
C5b—N7b—Pt		123.7(6)
C8b—N7b—Pt		130.6(6)
base a/coord plane N₂P₂ (deg)	80.6(2)	79.5(1)
base b/coord plane N₂P₂ (deg)	79.8(2)	86.25(1)
base a/base b (deg)	77.7(2)	76.99(1)

[a] N3a,b refers to **4b** and N7a,b to **5b**.

each base ring and a phenyl group [base a—phenyl C3, centroid-to-centroid distance 3.480(6) Å; base b—phenyl C21, 3.448(7) Å]. In **5b**, the intramolecular π—π interaction between the imidazole ring of base b and phenyl C21 is even present [centroid-to-centroid distance 3.488(7) Å]. On the other hand, the different conformation assumed by the phosphine P1, leading the methyl group C1 to lay approximately in the coordination plane (Figure 6), induces a weaker π—π stacking linking the phenyl groups C3 and C15 [distance 3.784(7) Å]. In the solid-state structure, a hydrogen-bonding interaction of type C—H···O between a phenyl group and the guanine oxygen O6 in **3a** (O6b in **5b**) is also present. The C···O distances are 3.361(11) and 3.246(13) Å, respectively. All of these interactions are likely to stabilize the crystal packing and the solid-state conformations of these complexes. It is worth noting the crystal packing of **5b**, where each guanine is connected through hydrogen bonds via amino group N2 and nitrogen N3 of the centrosymmetric moiety, forming a mismatched homo base pairing [NH₂···N = 3.03 Å (base a) and 2.98 Å (base b)].[18] The atoms of the two nucleobases are coplanar within ±0.03 and ±0.02 Å in **4b** and **5b**), respectively. Moreover, N1 and N2 nitrogen atoms act as hydrogen-bond donors toward a nitrate. Figure 7 shows the hydrogen-bonding pattern, which gives rise to a zigzag complex polymer with pendant nitrate anions.

3. NMR Characterization of *cis*-[L₂Pt(nucleobase)-(ONO₂)]⁺ and *cis*-[L₂Pt(nucleobase)₂]²⁺. In solution, the isolated bisadducts *cis*-[L₂Pt(nucleobase)₂]²⁺ do not manifest particular features. The ¹H and ³¹P NMR spectra of the isolated complexes, obtained in different solvents, show a single set of resonances indicative of the chemical equivalence of the two

(18) (a) Roitzsch, M.; Lippert, B. *Chem. Commun.* **2005**, 5991. (b) Freisinger, E.; Rother, I. B.; Lüth, M. S.; Lippert, B. *Proc. Natl. Acad. Sci. U.S.A.* **2003**, *100*, 3748. (c) Erxleben, A.; Metzger, S.; Britten, J. F.; Lock, C. J. L.; Albinati, A.; Lippert, B. *Inorg. Chim. Acta* **2002**, *339*, 461.
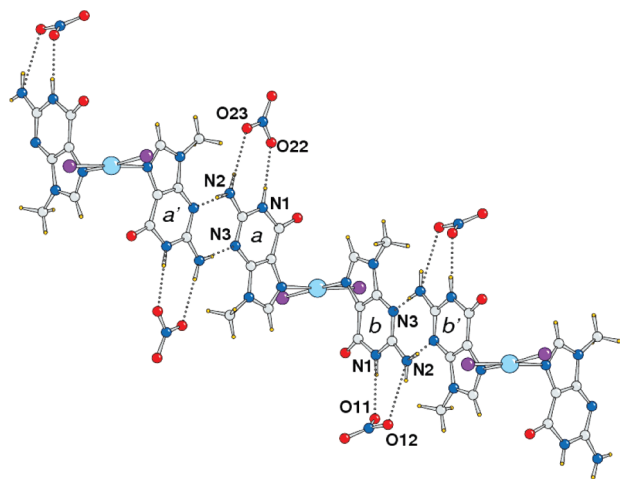
Figure 7. Crystal packing of **5b** showing the one-dimensional polymers built by hydrogen-bond interactions (dotted lines).
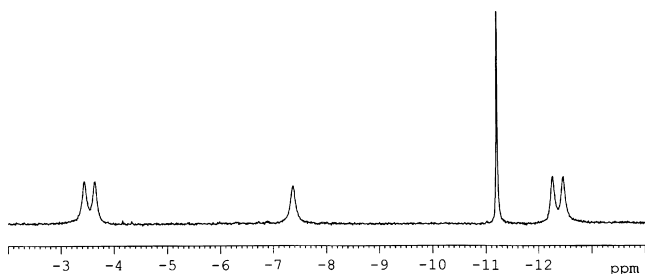

Figure 8. $^{31}P\{^1H\}$ NMR spectra in DMSO-d_6 (central part) of a mixture (0.1 M) of **1b** and **4b** (1:1).

Figure 9. $^{31}P\{^1H\}$ NMR spectra (central part) of **2a** in (a) DMSO-d_6, (b) DMF-d_7, and (c) CD_2Cl_2 and (d) an expansion of part c.

nucleobases. As previously noticed, the platination of the cytosine at the N3 site shifts at lower field the resonance of the exocyclic NH$_2$ protons, observed as broad singlets with the same relative intensities, at δ 9.04 and 7.93 ppm for L = PPh$_3$, in DMSO-d_6. Similarly, the platination of 9-MeGu at the N7 site, as confirmed through $^1H-^{15}N$ heterocorrelated spectra (see the Supporting Information), causes deshielding of the H1 proton, up to 0.8 ppm for **5a**.

The coordination of two nucleobases to cis-L$_2$Pt(ONO$_2$)$_2$ (in DMSO-d_6) determines an upfield shift of the ^{31}P NMR resonances and a decrease of the $^1J_{PPt}$ values. For 1-MeCy, the chemical shift differences ($\Delta\delta$) are 4.3 and 5.4 ppm for PMePh$_2$ and PPh$_3$, respectively, while for 9-MeGu $\Delta\delta$ are 2.4 and 3.1 ppm. As an example of the spectroscopic changes observed upon coordination of 1-MeCy to cis-(PMePh$_2$)$_2$Pt(ONO$_2$)$_2$, the ^{31}P NMR spectrum obtained immediately after dissolution of equimolar amounts of dinitrate and 1-MeCy, in DMSO-d_6 [or, alternatively, cis-(PMePh$_2$)$_2$Pt(ONO$_2$)$_2$ and cis-[(PMePh$_2$)$_2$Pt(1-MeCy)$_2$](NO$_3$)$_2$ in a 1:1 molar ratio] is shown in Figure 8.

The spectrum is characterized by two AX doublets ($^2J_{PP}$ = 24.3 Hz) with the same relative intensity, at δ −12.36 ppm ($^1J_{PPt}$ = 3934 Hz) and δ −3.54 ppm ($^1J_{PPt}$ = 3453 Hz), attributed to the monoadduct cis-[(PMePh$_2$)$_2$Pt(1-MeCy)]$^{2+}$, a broad singlet at δ −6.90 ppm of unreacted **1b**, and a sharp singlet at δ −11.13 ppm ($^1J_{PPt}$ = 3322 Hz) due to the bisadduct **4b**. This last signal is the only detectable one when an additional equiv of nucleobase is added, while the initial AX multiplet disappears immediately. The doublet at lower
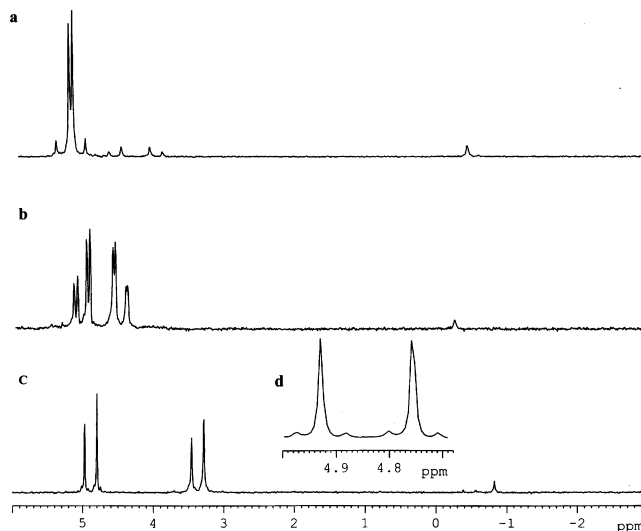
field in Figure 8, having $^1J_{PPt}$ = 3934 Hz, can be assigned to the phosphine trans to the nitrate ligand or, more likely, to a solvent molecule. The upfield doublet, with $^1J_{PPt}$ = 3453 Hz, consequently is attributable to the phosphine trans to the nucleobase. Similar results were obtained with 9-MeGu (in DMSO-d_6: δ −11.46 ($^1J_{PPt}$ = 3870 Hz), −2.72 ($^1J_{PPt}$ = 3430 Hz, with $^2J_{PP}$ = 23.4 Hz).

For both of the nucleobases investigated, the monoadducts cis-[L$_2$Pt(nucleobase)]$^{2+}$ (L = PMePh$_2$) are in equilibrium with relatively high concentrations of the bisadducts cis-[L$_2$Pt(nucleobase)$_2$]$^{2+}$ (and dinitrate). Thus, from the relative intensities of the signals in Figure 8, cis-[(PMePh$_2$)$_2$Pt(1-MeCy)]$^{2+}$ accounts for 63% of all of the phosphine-containing species. However, when L is PPh$_3$, the relative stability of the monoadducts **2a** and **3a** appears largely increased. In Figure 9a, the ^{31}P NMR spectrum of a solution of ca. 0.1 M of **2a** in the DMSO-d_6 is shown. The bisadduct **4a**, in equilibrium with the monoadduct, is observed as a singlet at δ −0.81 ppm and its relative intensity is about 4%. The resonance due to cis-(PPh$_3$)$_2$Pt(NO$_3$)$_2$ is undetectable, being overlapped with those of the monoadduct, characterized by two AB multiplets.

The main resonances, at δ 5.36 ($^1J_{PPt}$ = 4080 Hz) and 5.12 ($^1J_{PPt}$ = 3536 Hz), with $^2J_{PP}$ = 22.3 Hz, can be assigned to the solvent complex cis-[(PPh$_3$)$_2$Pt(1-MeCy)(DMSO)]$^{2+}$, while the weaker multiplets δ 4.60 and 4.02 ($^2J_{PP}$ = 21.4 Hz) are attributable to the species cis-[(PPh$_3$)$_2$Pt(1-MeCy)(ONO$_2$)]$^+$ in which the nitrate ion is in the coordination sphere of the metal, as found in the solid-state structure. The intensities of these latter signals, in fact, increase when the NO$_3^-$ ions are added (such as the Ph$_4$AsNO$_3$ salt). The unusually small chemical shift differences of the two phosphines ($\Delta\delta$ = 0.24 and 0.58 ppm), compared with that found for the PMePh$_2$ analogue ($\Delta\delta$ = 8.82 ppm; Figure 8), can be accounted for by the presence of strong intraligand $\pi-\pi$ interactions, as are found in the solid state, which prevent the free rotation around the Pt−P and/or Pt−N3 bonds. The imposed rigidity causes a strong chemical shift

anisotropy and a consequent shift at lower field of one of the phosphine resonances.[19]

Similar considerations apply to the ^{31}P NMR spectrum of **2a** in DMF. As shown in Figure 9b, two AB multiplets have almost the same relative intensity and very similar chemical shifts (see the Experimental Section). These data suggest the presence of the solvent complex *cis*-[(PPh$_3$)$_2$Pt(1-MeCy)-(DMF)]$^{2+}$ in which the DMF and the nucleobase are arranged in different conformations on the coordination plane of the metal. The resonances at lower field, having higher values of $^1J_{PPt}$ (4015 Hz), are assigned to the PPh$_3$ trans to the DMF ligand.

A different pattern of the ^{31}P NMR spectrum is observed in chlorinated solvents. Figure 9c refers to a solution of **1a** and 1-MeCy (ca. a 1:1.1 molar ratio) in CD$_2$Cl$_2$. In addition to the singlets at δ −0.61 and +3.49 ppm, due to species **4a** and **1a**, respectively, the spectrum is characterized by two AX doublets ($^2J_{PP}$ = 21.3 Hz) at δ 5.11 ($^1J_{PPt}$ = 3939 Hz) and 3.58 ppm ($^1J_{PPt}$ = 3455 Hz) having slightly different line widths. The doublet at higher field, on the basis of its lower value of $^1J_{PPt}$, is assigned to the phosphine trans to the N3-coordinated cytosine. This signal is overlapped with the singlet due to unreacted **1a**. The resonance centered at δ 5.11 ppm exhibits a $^1J_{PPt}$ value (3939 Hz) typical for a phosphine trans to an oxygen donor ligand. Moreover, this doublet is characterized by very weak satellites (separation of ca. 11 Hz; Figure 9d) likely due to long-range ^{31}P−^{195}Pt coupling. Such satellites, although less resolved, are detectable also for the doublet at higher field and suggest the presence of a polynuclear species in which the neutral nucleobase acts as a bidentate bridging ligand likely through the N3 and O2 atoms. Attempts to grow crystals of **2a** from chlorinated solvents in order to prove this unusual binding mode were unsuccessful.

Although in the solid state complexes **2a** and **3a** exhibit strong analogies, in solution they disclose important differences. The ^{31}P NMR spectrum of **3a** in DMSO-d_6 shows a single set of resonances (AB multiplet at δ 7.94 and 5.12 ppm) indicative of a *complete* solvolysis of the nitrate Pt−O bond. Moreover, the multiplicity of signals observed in a DMF solution (see the Experimental Section) points to the presence of other species in equilibrium, in addition to that found in the solid state and the solvent complex, *cis*-[(PPh$_3$)$_2$Pt(9-MeGu-N^7)(DMF)]$^{2+}$. The relatively high difference between the two chemical shift values ($\Delta\delta$ = 2.88 ppm) could be assigned to the chelated complex *cis*-[(PPh$_3$)$_2$Pt(9-MeGu-N^7O^6)]$^{2+}$ in which the nucleobase binds the metal through the N7 and O6 atoms, a coordination mode

for the 9-substituted guanines unprecedented for platinum(II). The spectroscopic parameters of this species, which is the main component of the equilibrium mixture (ca. 60%), are similar to those of the species found in DMSO. The addition of 1 equiv of 9-MeGu to the DMF or DMSO solution of **3a** affords the immediate formation of the bisadduct **5a** in quantitative yield (by NMR).

Conclusions

The coordination of two molecules of 1-MeCy and 9-MeGu to the metal center of *cis*-L$_2$Pt(ONO$_2$)$_2$ (L = PPh$_2$Me, PPh$_3$) appears kinetically facile, as expected for the presence of good leaving groups, such as the NO$_3^-$ ligands. The stereochemistry of the bisadducts *cis*-[L$_2$Pt-(nucleobase)$_2$]$^{2+}$ (L = PMePh$_2$) is that of a *head-to-tail* arrangement of the two cytosines and guanines, N3- and N7-coordinated, respectively. The X-ray structures confirm that the two nucleobases do not determine steric crowding in the metal coordination sphere (the sums of bond angles P−Pt−P and N−Pt−N are 179.2° and 180.6° in **4b** and **5b**, respectively). Despite the apparent thermodynamic stability of the corresponding PPh$_3$ analogues, we were unable to crystallize the complexes *cis*-[(PPh$_3$)$_2$Pt(nucleobase)$_2$]$^{2+}$ (**4a** and **5a**), a failure likely related to the higher steric requirements of the PPh$_3$ (cone angles of 145° and 136° for L = PPh$_3$ and PMePh$_2$, respectively).[20] It is worth noting that in the strictly related bisadduct *cis*-[(PPh$_3$)$_2$Pt(1-MeCy-N^3)(1-MeCy(-H)-N^4)]NO$_3$, containing a neutral and a NH$_2$-deprotonated cytosine, the P−Pt−P and N3−Pt−N4 angles are 98.22(4)° and 87.51(13)°, respectively.[6] The platination of both cytosines at the N3 atom (or the guanine at N7) was expected to further increase such deviations from the ideal value of 90°.

Finally, the relatively high stability of the monoadducts *cis*-[L$_2$Pt(nucleobase)]$^{2+}$ when L = PPh$_3$ ligands can be accounted for by the presence in both complexes of a strong intramolecular π−π interaction occurring between a phenyl group and the pyrimydinic (or purinic) ring, which leads the P−Pt−N3/7 angle to assume a value near to ideality.

Supporting Information Available: Crystallographic data in CIF format for the structures reported in this paper and ^{15}N−^1H HMBC spectra of **5a** in DMSO-d_6. This material is available free of charge via the Internet at http://pubs.acs.org.

IC7020319

(19) Garrou, P. E. *Chem. Rev.* **1977**, *77*, 313.

(20) Tolman, C. A. *Chem. Rev.* **1981**, *81*, 229.